Journal of Inflammation Research

Dovepress
Taylor & Francis Group

Open Access Full Text Article

ORIGINAL RESEARCH

Chinese Medicine Formula HJ11 Alleviates Atherosclerosis by Inactivating the TLR4/MyD88/IκB-α Pathway and Modulating the Heart-Gut Axis Response

Fangyuan Zhang[1,*], Fei Lu[2,*], Mingfei Shi[3], Weiming Xu[4], Ziyun Li[5], Yuting Cui[6], Jiaxi Zou[7], Jingqing Hu[8]

[1]School of Pharmaceutical Science and Technology, Hangzhou Institute for Advanced Study, University of Chinese Academy of Sciences, Hangzhou, Zhejiang, People's Republic of China; [2]Department of Traditional Chinese Medicine, Liaoning University, Shenyang, Liaoning, People's Republic of China; [3]School of Integrated Chinese and Western Medicine, Nanjing University of Chinese Medicine, Nanjing, Jiangsu, People's Republic of China; [4]China Science and Technology Development Center for Chinese Medicine, Beijing, People's Republic of China; [5]School of Acupuncture and Tuina, School of Regimen and Rehabilitation, Nanjing University of Chinese Medicine, Nanjing, Jiangsu, People's Republic of China; [6]Department of Cardiology, Affiliated Hospital of Nanjing University of Chinese Medicine, Nanjing, Jiangsu, People's Republic of China; [7]School of Clinical Medicine, School of Basic Medical Sciences, Chengdu University of Traditional Chinese Medicine, Chengdu, Sichuan, People's Republic of China; [8]School of Traditional Chinese Medicine, Tianjin University of Traditional Chinese Medicine, Tianjin, People's Republic of China

*These authors contributed equally to this work

Correspondence: Jingqing Hu, School of Traditional Chinese Medicine, Tianjin University of Traditional Chinese Medicine, Tianjin, People's Republic of China, Tel/Fax +86-139-1154-6633, Email gcp306@126.com

Journal of Inflammation Research downloaded from https://www.dovepress.com/
For personal use only.

Background: Extensive research has demonstrated that gut microbiota and its metabolites—including short-chain fatty acids, trimethylamine N-oxide (TMAO), and bile acids—play a crucial role in the pathophysiology of coronary artery disease (CAD).The bidirectional interaction between the gut microbiota and the cardiovascular system significantly influences host metabolic and inflammatory homeostasis. As a result, targeted modulation of the gut microbiota emerges as a promising adjunctive therapeutic strategy for CAD, offering potential benefits with minimal side effects.

Purpose: This study aims to elucidate the therapeutic mechanisms of the clinically validated Chinese medicine formula HJ11 in mitigating coronary heart disease (CHD), with a particular focus on its regulation of the heart-gut axis and associated atherosclerotic processes.

Study Design and Methods: This study established an ApoE−/− mouse model of atherosclerosis and treated with HJ11 via gavage. We investigated the effects of HJ11 on the gut microenvironment in these atherosclerotic mice. Gut microbial composition and faecal metabolite profiles were analyzed using 16S rDNA sequencing and metabolomics. Additionally, an in vitro model of atherosclerosis was used to examine whether HJ11 exerts anti-inflammatory effects by modulating the TLR4/MYD88/IκB-α signaling pathway.

Results: HJ11 exerted protective effects on coronary atherosclerosis by reducing systemic serum lipid levels and inhibiting plaque formation, vascular inflammation, and collagen deposition, while also alleviating aortic injury. It suppressed endothelial inflammation and inhibited the proliferation of vascular smooth muscle cells. In the gut, HJ11 alleviated intestinal structural damage and enhanced barrier integrity. Notably, it promoted the function of Akkermansia, a beneficial bacterium known to influence TLR4 expression. Finally, in an in vitro atherosclerosis model, HJ11 decoction inhibited cell proliferation and migration by inactivating the TLR4/MYD88/IκB-α signaling pathway—an effect that was abolished by TLR4 overexpression.

Keywords: HJ11 formula, atherosclerosis, inflammation, intestinal barrier, heart-gut axis

Introduction

Atherosclerosis is a chronic inflammatory disease of the arteries and a major contributor to cardiovascular conditions. It is marked by plaque buildup within arterial walls,[1] when this plaque ruptures, it can lead to thrombosis, vascular

Received: 17 February 2025
Accepted: 4 December 2025
Published: 11 December 2025

© 2025 Zhang et al. This work is published and licensed by Dove Medical Press Limited. The full terms of this license are available at https://www.dovepress.com/terms.php and incorporate the Creative Commons Attribution – Non Commercial (unported, v4.0) License (http://creativecommons.org/licenses/by-nc/4.0/). By accessing the work you hereby accept the Terms. Non-commercial uses of the work are permitted without any further permission from Dove Medical Press Limited, provided the work is properly attributed. For permission for commercial use of this work, please see paragraphs 4.2 and 5 of our Terms (https://www.dovepress.com/terms.php).

blockage, and life-threatening events such as stroke and heart attacks.[2,3] Risk factors include genetic predisposition, hypertension, hypercholesterolemia, and unhealthy lifestyle habits such as poor diet, high-fat diet, alcohol consumption, and smoking. Additionally, the gut microbiota plays a role in atherosclerosis through its metabolites that modulate inflammation.[4,5] Despite advances in treatment, atherosclerosis remains a leading cause of death globally.[6] Therefore, identifying effective therapeutic agents is an urgent priority.

In recent years, traditional Chinese herbal medicine has demonstrated notable advantages in the treatment of atherosclerosis.[7] The Si-Miao-Yong-An formula, originally used to treat gangrene, has recently shown efficacy in managing cardiovascular diseases.[8] Notably, it has been effective in treating atherosclerosis by reducing lipid deposition, cholesterol crystallization, pro-inflammatory factor secretion, and plaque size in ApoE−/− mice.[9,10]

HJ11 is a clinically effective formula derived from the traditional Si Miao Yong An Tang, with additional herbal components. The original formula includes Salvia miltiorrhiza Bge (Dan Shen; root), Forsythia suspensa (Thunb), Vahl (Lian Qiao; fruit), Ramulus Cinnamomi (Gui Zhi; stem), and Reynoutria japonica Houtt (Hu Zhang; root). In HJ11, additional herbs such as Lonicera japonica Thunb (Jin Yin Hua; flower), Scrophularia ningpoensis Hemsl (Xuan Shen; root), Glycyrrhiza uralensis (Sheng Gan Cao; root), and Angelica sinensis (Oliv). Diels (Dang Gui; root) are incorporated. This formula is patented (Patent No. ZL202210933899.7). The HPLC profiles of the herbal components used in this study are provided in the supplementary materials (Figure S1). HJ11 formula has been evaluated in multiple exploratory clinical trials for various cardiovascular conditions, including unstable angina (CHiCTR2100043038), non-ST segment elevation myocardial infarction (CHiCTR2100043057), and arteriosclerosis obliterans (CHiCTR2100043056). These studies have demonstrated that HJ11 can improve cardiac function and alleviate vascular damage in patients, supporting its therapeutic potential in atherosclerosis-related diseases.

Previous studies have shown that HJ11 reduces cardiac injury in rats with acute myocardial infarction by modulating intestinal microbiota and their metabolites.[11] It also alleviates myocardial ischemia/reperfusion injury by inhibiting ferroptosis.[12] However, the specific mechanisms underlying its protective effects in atherosclerosis remain unclear.It is well established that both inflammation and gut microbiota-derived metabolites are key contributors to cardiovascular diseases, including atherosclerosis.[13] Recent clinical trials have demonstrated that targeting inflammation not only prevents atherosclerosis progression but also improves patient outcomes. Accordingly,anti-inflammatory strategies such as suppression of pro-inflammatory cytokines and inhibition of inflammatory signaling pathways have gained attention in atherosclerosis treatment.[14,15] In parallel, accumulating evidence indicates that gut microbiota regulate intestinal function, nutrient absorption, and lipid metabolism. Dysbiosis has been linked to impaired lipid handling and increased systemic inflammation via toxic metabolite release, thereby accelerating atherosclerosis.[13,16] Thus, restoring gut microbial balance represents a promising approach for atherosclerosis prevention and therapy.[17] Given the anti-inflammatory and microbiota-regulating effects of HJ11,[5,18] we hypothesized that HJ11 may exert therapeutic effects on atherosclerosis and therefore explored its potential mechanisms in this context.

The toll-like receptor 4 (TLR4)/myeloid differentiation factor-88 (MYD88)/IκB-α signaling pathway is a key mediator of immune inflammation and has been shown to influence vascular endothelial inflammation, thereby contributing to atherosclerosis progression.[19] Moreover, this pathway is also involved in regulating gut microbial diversity.[20] Whether HJ11 modulates the cardio-intestinal axis by targeting TLR4 signaling to attenuate atherosclerotic damage is the central question of this study.In our preliminary experiments, we established an atherosclerosis cell model by treating mouse aortic vascular endothelial cells with lipopolysaccharide (LPS). HJ11 treatment significantly suppressed activation of the TLR4/MYD88/IκB-α pathway in this model. Based on these findings, the present study aims to further investigate the regulatory effects of HJ11 on this signaling pathway in the context of atherosclerosis, with a particular focus on gut microbiota-mediated mechanisms.

Materials and Methods

Preparation of HJ11 Formula

The Chinese herbal pieces of the HJ11 formula were purchased from CR SANJIU Pharmaceutical Co., Ltd. (Hefei, Anhui, China, Chinese Pharmacopoeia, 2020). A total of 102 g of crude herbal materials was mixed and soaked in

500 mL of distilled water at room temperature for 30 minutes. The soaked mixture was then decocted at atmospheric pressure by bringing it to a boil over high heat, followed by simmering over low heat for 30 minutes. The herbal residue was subsequently subjected to a second decoction with an additional volume of distilled water, boiled again and simmered over low heat for 15 minutes. The two extracts were combined and concentrated to a final concentration of 2.0 g/mL. The resulting decoction was allowed to cool to room temperature and then stored at 4 °C until use.The determination results of compounds in the components related to this formula were presented in the Table S1.

Construction of the ApoE−/− Mouse Model of Atherosclerosis

A total of 27 male ApoE−/− mice (8 weeks old, weighing 20–25 g), along with 9 male C57BL/6J mice (8 weeks old, weighing 20–25 g), were purchased from Zhongke Zesheng Technology Co. (Beijing, China). All mice were acclimatized for one week in a room with a 12 - hour light/dark cycle (at 22°C), and were free from specific pathogens. Food and water were provided ad libitum. Animal experiments in the current study were approved by the Animal Ethics Committee of Beijing Maidekangna Biotechnology Co., Ltd. (Approval No. MDKN-2022-086), and all procedures were conducted in accordance with the Guidelines for the Care and Use of Laboratory Animals, the ethical standards of the Committee, and the national regulations of China.

Following one week of acclimation, the 27 ApoE−/− mice were randomly divided into the ApoE−/− group (n = 9), the HJ11-L group (n = 9), and the HJ11-H group (n = 9). The sample size was determined based on previous studies investigating atherosclerotic models and herbal interventions, where 6–9 animals per group were typically used to detect significant differences in key outcomes.[21,22]

The C57BL/6J mice served as the Control group (n = 9) and were fed a normal chow diet for 18 weeks. The ApoE−/− group was fed a high-fat diet for 18 weeks. For the HJ11-L and HJ11-H groups, the mice were given a high-fat diet for 18 weeks; from weeks 10 to 18, the HJ11 formula was administered by gavage at a low dose (6.63 g/kg/day, equivalent to the normal clinical minimum dose, once daily) and a high dose (13.26 g/kg/day, equivalent to the normal clinical maximum dose, once daily) to the ApoE−/− mice in the HJ11-L and HJ11-H groups, respectively. The high-fat diet was purchased from Harlan Teklad (TD08028, Madison, WI, USA).

On the last day of the experiment, the food intake of each mouse was recorded. On the second day after the final administration of HJ11 formula, the body weight of each mouse was measured, followed by blood collection from the eyeballs. Subsequently, all mice were euthanized. The aortic root was carefully dissected and divided into segments: one portion was fixed in 4% paraformaldehyde for histological analyses, and another portion was snap-frozen in liquid nitrogen and stored at −80°C for RNA extraction (qRT-PCR). The entire aorta and intestine were collected and stored at −80°C.

Blood Sample and Biochemistry Test

Blood samples collected from the eyeballs of mice collected and aliquoted into 6 tubes (20–30 μL each) and stored at −80°C, with each aliquot used for only one assay to avoid repeated freeze-thaw cycles. After centrifugation at 3000 rpm for 10 minutes at 4°C, the levels of total cholesterol (TC), triglycerides (TG), low-density lipoprotein (LDL), and high-density lipoprotein (HDL) in the supernatant were measured using the Catalyst One Chemistry Analyzer (IDEXX Laboratories Inc., Westbrook, ME, USA), following the manufacturer's instructions.

Oil Red O Staining

The entire aorta of each mouse was subjected to Oil Red O staining to detect the atherosclerotic plaque area. Aortic tissues were fixed in 4% formaldehyde solution (Beyotime, Shanghai, China) for 10 minutes at 4°C, followed by rinsing in 60% isopropanol (Guangfu Fine Chemical Research Institute, Tianjin, China) for 10 minutes. The tissues were then stained with 0.05% Oil Red O solution (Beyotime, Shanghai, China) for 20 minutes. After sequential washing with 60% isopropanol and water, the tissues were placed on glass slides with the endothelial surface facing up. The aortic lesion area,specifically the plaque area, was photographed using a digital camera (Nikon, Tokyo, Japan) and quantified using ImageJ software (version 1.46r, NIH, Bethesda, MD, USA). The degree of atherosclerosis was evaluated using the formula: (aortic lesion area / total aortic area) × 100%.

Hematoxylin and Eosin (HE) Staining and Alcian Blue Staining

The root of the aorta and the intestine of the mice were fixed in 4% paraformaldehyde (Beyotime, Shanghai, China) for 24 hours, then embedded in paraffin and sectioned into 5 μm thick slices. The sections were deparaffinized with xylene (Guangfu Fine Chemical Research Institute, Tianjin, China) for 10 minutes, followed by rehydration in a series of decreasing alcohol gradients (Guangfu Fine Chemical Research Institute, Tianjin, China). Hematoxylin staining solution (Beyotime, Shanghai, China) was applied to stain the sections for 5 minutes at room temperature. After rinsing with running water, the sections were differentiated in 5% acetic acid (Guangfu Fine Chemical Research Institute, Tianjin, China) for 1 minute at room temperature. Eosin staining solution (Beyotime, Shanghai, China) was then used to stain the sections for 1 minute at room temperature. After washing with running water, the sections were dehydrated through a series of increasing alcohol gradients and xylene. The sections were then mounted in neutral resin and observed under an optical microscope (Olympus, Tokyo, Japan). Intestinal damage was assessed, and the lesion area of the aortic root was quantified. Vascular pathology was evaluated using the formula: (lesion area / total aortic area) × 100%.

For Alcian blue staining, after rehydration, the intestinal sections were stained with Alcian blue solution (Solarbio, Beijing, China) for 15 minutes. The sections were then dehydrated, dried, and examined under an optical microscope (Olympus, Tokyo, Japan) to count the number of goblet cells.

Masson Staining

Collagen deposition in the aortic root plaque was assessed using Masson staining. As described for HE staining, the aortic root sections were prepared, deparaffinized, and rehydrated. The sections were first stained with hematoxylin for 5 minutes, then differentiated in 1% hydrochloric acid alcohol (Beyotime, Shanghai, China) for 10 seconds. After rinsing with running water, the sections were stained with Ponceau staining solution (Beyotime, Shanghai, China) for 5 minutes. The sections were then washed with distilled water. Phosphomolybdic acid solution (Yuanye Biotechnology, Shanghai, China) and aniline blue staining solution (Solarbio, Beijing, China) were sequentially applied for 5 minutes each. After treatment with 1% acetic acid (Jieshikang Biotechnology, Qingdao, China) for 1 minute, the sections were dehydrated, dried, and mounted. The collagen deposition area (positive Masson staining area) was quantified using the formula: (positive Masson staining area / lesion area) × 100%. The sections were then observed under an optical microscope (Olympus, Tokyo, Japan).

Enzyme-Linked Immunosorbent Assay (ELISA)

ELISA was used to detect changes in serum cytokine levels in mice. Briefly, blood samples were centrifuged at 3000 rpm for 10 minutes at 4°C. The levels of interleukin-6 (IL-6), interleukin-1β (IL-1β), vascular cellular adhesion molecule-1 (VCAM-1), tumor necrosis factor-α (TNF-α), matrix metalloproteinase-9 (MMP-9), and lipopolysaccharide (LPS) in the supernatant were measured according to the manufacturer's instructions. Intestinal LPS, a major component of the outer membrane of Gram-negative bacteria naturally present in the gut microbiota, was measured to evaluate intestinal inflammation and barrier integrity.[23] The following commercial kits were used: IL-6 assay kit (Kanglang Biotechnology, Shanghai, China), IL-1β assay kit (JingKang Bioengineering, Shanghai, China), VCAM-1 assay kit (Kanglang Biotechnology, Shanghai, China), TNF-α assay kit (JingKang Bioengineering, Shanghai, China), MMP-9 assay kit (JingKang Bioengineering, Shanghai, China), and LPS assay kit (Zhenke Biotechnology, Shanghai, China).

Additionally, LPS levels in the intestine were measured. The intestine was dissected into small pieces, ground in lysate (Yuanye Biotechnology, Shanghai, China) on ice to form a tissue homogenate, and centrifuged at 15,000 rpm for 10 minutes at 4°C. LPS levels in the supernatant were then assessed using the LPS assay kit (Zhenke Biotechnology, Shanghai, China).

Intestinal Permeability Assay

At the end of the experiment, mice in each group were administered 4-kDa fluorescein isothiocyanate (FITC)-dextran (Biolab Technology, Beijing, China) by gavage at a dose of 500 mg/kg. After 4 hours, blood samples were collected from

the eyeballs and centrifuged at 3000 rpm for 10 minutes at 4°C. The FITC-dextran level in the serum was measured by detecting fluorescence intensity using a spectrophotometer (excitation: 492 nm; emission: 525 nm).

Immunohistochemistry

Immunohistochemistry was performed on the aortic root of mice to explore TLR4 expression. The aortic root was sequentially immobilized, paraffin-embedded, sectioned, deparaffinized, and rehydrated as described in the HE staining method. The sections were then incubated in 3% H_2O_2 for 10 minutes, boiled in citrate buffer for 3 minutes, and blocked with normal goat serum (Beyotime, Shanghai, China) for 30 minutes. Rabbit anti-TLR4 primary antibody (1:100, GH0836, Biolab Technology, Beijing, China) was applied overnight at 4°C. After washing off the excess primary antibody with phosphate-buffered saline, the sections were incubated with horseradish peroxidase-labeled goat anti-rabbit secondary antibody (1:200, WK355, Biolab Technology, Beijing, China) for 1 hour. The sections were then reacted with 3,3′-diaminobenzidine (Beyotime, Shanghai, China) for 5 minutes and counterstained with hematoxylin solution for 1 minute. Finally, the sections were dehydrated, dried, and sealed. TLR4-positive staining was observed under an optical microscope (Olympus, Tokyo, Japan) and quantified using Image J software (ImageJ, NIH, Bethesda, MD, USA). The percentage of TLR4-positive area was calculated as (TLR4-positive staining area/total aorta area) × 100%.

Real-Time Quantitative Reverse Transcription-Polymerase Chain Reaction (qRT-PCR)

Total RNA was extracted from the aortic root and intestine of mice using TRIzol reagent (Biolab Technology, Beijing, China) according to the manufacturer's instructions. Reverse transcription was performed with the total RNA samples to synthesize cDNA using PrimeScript RT Master Mix (TaKaRa, Tokyo, Japan). Subsequently, qRT-PCR was carried out using the SYBR Premix Ex Taq kit (TaKaRa, Tokyo, Japan) on the iCycler instrument (Bio-Rad Laboratories, Hercules, CA, USA). The PCR conditions were as follows: 95°C for 30s, followed by 40 cycles of 95°C for 5s, 55°C for 30s, and 72°C for 60s. The primers used were:

TLR4:Forward,5′-CTGGGTGAGAAAGCTGGTAA-3′,Reverse,5′-AGCCTTCCTGGATGATGTTGG-3′

NF-κB:Forward,5′-CCAAAGAAGGACACGACAGAATC-3′,Reverse,5′-GGCAGGCTATTGCTCATCACA-3′

Occludin:Forward,5′-TGAAAGTCCACCTCCTTACAGA-3′,Reverse,5′-CCGGATAAAAAGAGTACGCTGG-3′

ZO-1:Forward,5′-GCCGCTAAGAGCACAGCAA-3′,Reverse,5′-GCCCTCCTTTTAACACATCAGA-3′

Claudin-3:Forward,5′-ACCAACTGCGTACAAGACGAG-3′,Reverse,5′-CGGGCACCAACGGGTTATAG-3′

β-actin:Forward,5′-AGCTTACTGCTCTGGCTCCTAGC-3′,Reverse,5′-ACTCATCGTACTCCTGCTTGCT-3′

mRNA expression levels of TLR4, NF-κB p65, Occludin, ZO-1, and Claudin-3 were calculated using the 2-ΔΔCT method, with β-actin as the reference gene.

Transmission Electron Microscopy (TEM)

The intestines of mice were fixed in 4% paraformaldehyde for 24 hours, followed by treatment with 1% buffered osmium tetroxide (Zhenzhun Biotechnology, Shanghai, China) for 1 hour. The tissues were then paraffin-embedded and sectioned into ultra-thin slices (50 nm thick). The sections were stained sequentially with uranyl acetate (Yubo Biotechnology, Shanghai, China) and lead citrate (Zhongjing Technology, Beijing, China). Finally, the sections were examined under a transmission electron microscope (TEM, JEM-1200EX, JEOL, Tokyo, Japan).

Cell Culture, Treatment, and Transfection

Mouse aortic vascular endothelial cells were obtained from Kanglang Biotechnology (Shanghai, China). The cells were cultured in Endothelial Cell Medium (ECM, Solarbio, Beijing, China), supplemented with 10% fetal bovine serum (FBS, Solarbio, Beijing, China), 1% endothelial cell growth factors (Solarbio, Beijing, China), and 1% penicillin/streptomycin (Solarbio, Beijing, China) at 37°C with 5% CO_2.

To establish the atherosclerosis cell model, mouse aortic vascular endothelial cells were treated with LPS at a final concentration of 100 ng/mL. To determine the optimal concentration of the HJ11 formula, the cells were co-treated with LPS (100 ng/mL) and varying concentrations of HJ11 formula (50, 100, 200, 400, 600, 800, and 1000 μg/mL) for 48 hours at 37°C with 5% CO_2.

pcDNA vectors carrying the TLR4 overexpression sequence and the corresponding negative control vectors were commercially obtained from GeneChem Technology (Shanghai, China). Mouse aortic vascular endothelial cells were seeded into 6-well plates at a density of 1×10^5 cells per well in

1 mL of serum-free ECM. The two types of vectors were transfected into the cells according to the manufacturer's instructions using Lipofectamine 3000 (Thermo Fisher Scientific, San Jose, CA, USA). Following transfection, the cells were treated with LPS (100 ng/mL) and HJ11 formula (50 μg/mL) for 48 hours at 37°C with 5% CO_2. Unstimulated mouse aortic vascular endothelial cells were used as the control.

Cell Counting Kit-8 (CCK-8) Assay

Mouse aortic vascular endothelial cells were seeded into 96-well plates at a density of 5×10^3 cells per well and cultured in the appropriate medium for 48 hours at 37°C with 5% CO_2. Subsequently, the cells were incubated with 10 μL of CCK-8 reagent (Solarbio, Beijing, China) for 2 hours at 37°C. To assess cell proliferation, the optical density (OD) values of the wells were measured at a wavelength of 450 nm using a microplate reader (Biotek, Winooski, VT, USA).

Transwell Experiment

Mouse aortic vascular endothelial cells (MAECs) were seeded into the upper chambers of Transwell plates with an 8 μm pore size. A total of 1×10^4 cells were plated in 200 μL serum-free endothelial cell medium (ECM) in each chamber. The lower chambers were filled with 500 μL ECM containing 20% fetal bovine serum (FBS) as a chemoattractant. The Transwell chambers were then incubated at 37°C with 5% CO_2 for 24 hours to allow cell migration. After incubation, the migrated cells were fixed with 4% paraformaldehyde for 15 minutes at room temperature. Following fixation, the cells were stained with 0.1% crystal violet for 10 minutes. The stained cells were observed under an inverted microscope (Olympus, Tokyo, Japan), and the number of migrated cells was counted in five randomly selected fields of view.

Cell Scratch Experiment

Mouse aortic vascular endothelial cells were seeded into 6-well plates at a density of 1×10^6 cells in 1 mL of ECM containing 10% FBS per well. After cell attachment, a scratch was made using a 10 μL pipette tip. The medium in each well was then replaced with 1 mL of serum-free ECM. The plates were incubated at 37°C with 5% CO_2 for 24 hours. The width of the scratch was observed under an inverted microscope (Olympus, Tokyo, Japan). The cell migration rate was calculated using the formula: ([original scratch width – final scratch width] / original scratch width) × 100%.

Western Blotting

Mouse aortic vascular endothelial cells were harvested after 48 hours of treatment under the relevant conditions. The cells were lysed in radio-immunoprecipitation assay (RIPA) buffer (Yuanye Biotechnology, Shanghai, China) containing a proteinase inhibitor and incubated for 30 minutes to extract total proteins. The lysed cells were then centrifuged at 12,000 rpm for 10 minutes at 4°C. The supernatant was analyzed for total protein concentration using the BCA Protein Assay kit (Beyotime, Shanghai, China) according to the manufacturer's instructions. Nuclear and cytoplasmic proteins were extracted using the Nucleoprotein & Cytoplasmic Protein Extraction Kit (AmyJet Scientific, Wuhan, China) following the provided protocol. Next, 50 μg of total proteins were separated by 10% sodium dodecyl sulfate-polyacrylamide gel electrophoresis (SDS-PAGE). After transfer to polyvinylidene fluoride (PVDF) membranes, the proteins were blocked in 5% skimmed milk for 2 hours at room temperature. The membranes were incubated with primary antibodies overnight at 4°C, followed by incubation with secondary antibodies for 2 hours at room temperature. Protein bands were visualized using an enhanced chemiluminescent reagent (Beyotime, Shanghai, China), and images were captured for further analysis. ImageJ software was used to quantify the proteins. Lamin B was used as a loading control for nuclear proteins, while β-actin served as a loading control for cytoplasmic and total proteins.

The primary antibodies used in this experiment were: rabbit anti-phosphorylated p65 (p-65) (1:1000, YT746, Biolab Technology, Beijing, China), rabbit anti-Lamin B (1:1000, ab16048, Abcam, Cambridge, UK), rabbit anti-TLR4 (1:1000, GH0836, Biolab Technology, Beijing, China), rabbit anti-Myeloid differentiation factor-88 (MYD88) (1:1000, ab133739, Abcam, Cambridge, UK),rabbit anti-phosphorylated IκB-α (p-IκB-α) (1:1000, AN371, Beyotime, Shanghai, China),

rabbit anti-IκB-α (IκB-α) (1:1000, 13,921–1, AmyJet Scientific, Wuhan, China), and rabbit anti-β-actin (1:1000, AF5003, Beyotime, Shanghai, China). A horseradish peroxidase-labeled goat anti-rabbit secondary antibody (1:2000, WK355, Biolab Technology, Beijing, China) was used for detection.

Immunofluorescence Staining

Immunofluorescence staining was performed to investigate the inflammation of macrophages and endothelial cells, as well as the proliferation of vascular smooth muscle cells (VSMC) in the aortic root. As described in the HE staining protocol, the aortic root tissue was prepared and rehydrated. After treatment with 0.5% Triton X-100 (Beyotime, Shanghai, China) for 20 minutes, the tissue was further blocked in normal goat serum for 30 minutes at room temperature. For double staining of p-p65/CD31, the tissue was incubated overnight at 4°C with rabbit anti-p-p65 primary antibody (1:100, YT828-TUV, Biolab Technology, Beijing, China) and mouse anti-CD31 primary antibody (1:100, ANT-051, AmyJet Scientific, Wuhan, China). Next, the tissue was treated with Alexa Fluor594-labeled goat anti-rabbit secondary antibody (1:200, 111-585-003, AmyJet Scientific, Wuhan, China) and Fluor488-labeled goat anti-mouse secondary antibody (1:200, 111-545-003, AmyJet Scientific, Wuhan, China) for 2 hours at room temperature.For α-smooth muscle actin (α-SMA)/CD68 double staining, rabbit anti-α-SMA primary antibody (1:100, ABP52852, AmyJet Scientific, Wuhan, China) and mouse anti-CD68 primary antibody (1:100, HM1070, AmyJet Scientific, Wuhan, China) were applied, followed by treatment with Alexa Fluor594-labeled goat anti-rabbit secondary antibody (1:200, 111-585-003, AmyJet Scientific, Wuhan, China) and Fluor488-labeled goat anti-mouse secondary antibody (1:200, 111-545-003, AmyJet Scientific, Wuhan, China). For ZO-1 immunofluorescence staining in the intestine, tissue was first stained with rabbit anti-ZO-1 primary antibody (1:200, YT771, Biolab Technology, Beijing, China) and then with Fluor488-labeled goat anti-rabbit secondary antibody (1:200, 111-545-045, AmyJet Scientific, Wuhan, China). After staining with 4′,6-diamidino-2-phenylindole (DAPI) (Beyotime, Shanghai, China) for 5 minutes in the dark, the tissues were dried, sealed, and observed under a fluorescence microscope (Olympus, Tokyo, Japan). The p-p65/CD31, α-SMA/CD68, and ZO-1 staining areas were quantified using ImageJ software.

Analysis of the Intestinal Microbiota

Fecal samples from mice were collected during the last three days of the experiment and stored at −80°C. Bacterial genomic DNA was extracted from these frozen fecal samples. PCR amplification was performed to amplify the V3 and V4 regions of the 16S rDNA gene. The primers used were: forward, 5′-ACTCCTACGGGAGGCAGCA-3′; reverse, 5′-GGACTACHVGGGTWTCTAAT-3′. The PCR products were subjected to high-throughput sequencing on the Illumina MiSeq platform (Biomarker Technologies, China). The raw paired-end reads from the original DNA fragments were first merged using FLASH32 and then assigned to each sample based on unique barcodes. Subsequently, basic analysis was performed using QIIME2 software. Specifically, the sequence tags were clustered into operational taxonomic units (OTUs) using the Usearch algorithm with a sequence similarity threshold of 97%. The number of OTUs shared by different groups was visualized using a Venn diagram. The α-diversity was assessed by analyzing the Chao1, Simpson, and Shannon indices using Mothur software. Taxonomic assignment of intestinal microbes was performed based on Phylum, Class, Order, Family, and Genus levels using QIIME software, and abundance charts were created using MicrobiomeAnalyst.Additionally, the metagenomeSeq method with R language software was used for metabolic pathway difference analysis. The linear discriminant analysis (LDA) effect size (LEfSe) method, based on the non-parametric factorial Kruskal–Wallis sum-rank test and the unpaired Wilcoxon rank-sum test, was applied to identify the most differentially abundant taxa. The LDA threshold was set to 2.6.

Liquid Chromatography-Mass Spectrometry (LC-MS)-Based Metabolomics Analysis

Fecal metabolites in mice were analyzed using a Dionex Ultimate 3000 RS UHPLC system (Thermo Fisher Scientific, San Jose, CA, USA) coupled with a Q-Exactive Plus Quadrupole-Orbitrap mass spectrometer equipped with a heated electrospray ionization (HESI) source. Briefly, 60 mg of each fecal sample were collected and placed into an Eppendorf tube containing two small steel balls. Internal standard (24 μL) and extraction solvent were added to each tube. The internal standard was prepared by dissolving 2-chloro-l-phenylalanine in methanol to a concentration of 0.3 mg/mL,

while the extraction solvent was a 4/1 (v/v) mixture of methanol and water. Quality control samples were prepared by pooling aliquots from all the samples. Each sample in the Eppendorf tube was then kept at −20°C for 5 minutes, ground for 2 minutes at 60 Hz, ultrasonicated for 10 minutes in cold water, and stored for 5 hours at −20°C. The mixture was subsequently centrifuged at 13,000 × g for 10 minutes at 4°C to collect the supernatant. For each supernatant sample, 150 μL was filtered through 0.22-μm microfilters. The filtered samples were then transferred to LC vials. The samples were analyzed using the Dionex Ultimate 3000 RS UHPLC, equipped with the Q-Exactive Plus Quadrupole-Orbitrap mass spectrometer and a heated electrospray ionization source. The mobile phase consisted of acetonitrile and water, both containing 0.1% formic acid. The parameters were as follows: column temperature, 45°C; flow rate, 0.35 mL/min; injection volume, 2 μL. The resolution was set to 70,000, with a mass range from *m/z* 100 to 1000, and collision energies of 10, 20, and 40 eV.The Progenesis QI software (v2.3) was used to process the original LC/MS data. Venn diagrams and Upset Venn diagrams were generated to show the number of fecal metabolites. Orthogonal Projections to Latent Structures Discriminant Analysis (OPLS-DA) was performed on the sample data using the Ropls package to distinguish differential metabolites. The differential metabolites were analyzed and compared with the differential genera.

Statistical Analysis

Data were obtained from three independently repeated experiments and processed into the form of mean ± standard deviation. GraphPad Prism software (Version 6.0) was applied for the statistical analysis. Prior to performing one-way analysis of variance (ANOVA), the assumptions of normality and homogeneity of variances were verified. Normality of data distribution for all outcome variables was assessed using the Shapiro–Wilk test. Homogeneity of variances across groups was confirmed using Levene's test. Then, ANOVA combined with Tukey's post hoc test, was used for the data comparison among multiple groups.

To address multiple comparisons in extensive biochemical and molecular analyses, Tukey's post hoc test was applied after one-way ANOVA to control the Type I error rate in pairwise group comparisons. Specifically, this approach was used for serum cytokine measurements, quantitative real-time PCR (qRT-PCR), and Western blotting data. For high-dimensional secondary analyses, such as fecal metabolomics involving multiple differential metabolites, the Benjamini–Hochberg procedure was employed to control the false discovery rate (FDR = 0.05), thereby minimizing the risk of false-positive results. $P < 0.05$ was deemed a statistically significantly difference.

Results

HJ11 Formula Blocked the Formation of Atherosclerotic Plaque in High-Fat Diet-Induced Atherosclerosis in ApoE−/− Mice

The experimental design for establishing the atherosclerosis model and the treatment protocol is illustrated in Figure 1A. Briefly, after one week of adaptive feeding, ApoE−/− mice of the ApoE−/− group, the HJ11-L group and the HJ11-H group were given high-fat diet for 18 weeks. At weeks 10–18, HJ11 formula at a low dose (6.63 g/kg/day) and a high dose (13.26 g/kg/day) were respectively administered to ApoE−/− mice of the HJ11-L group and the HJ11-H group by gavage. C57BL/6J mice of the Control group were given normal-chow-diet during the entire experimental period.

At the termination of the experiment, there was no statistically significant difference in body weight among the four groups of mice (Figure 1B). However, ApoE−/− mice of the ApoE−/− group had distinctly higher food intake than C57BL/6J mice of the Control group ($P < 0.05$). The difference in food intake among the ApoE−/− group and the two HJ11-H treatment groups was not statistically significant (Figure 1C). On the second day after the last administration, the blood samples were harvested from the eyeballs of mice. Serum biochemistry test showed the dramatically elevated serum levels of TC and LDL, but lower HDL level in ApoE−/− mice of the ApoE−/− group, by referring to the Control group ($P < 0.001$). As compared to the ApoE−/− group, ApoE−/− mice of the HJ11-L group had lower serum TC and LDL levels, but higher serum HDL level ($P < 0.05$, or $P < 0.01$). At the same time, ApoE−/− mice of the HJ11-H group exhibited lower serum levels of TC, TG and LDL, but higher serum HDL level than the ApoE−/− group ($P < 0.01$ or $P < 0.001$) (Figure 1D–G).

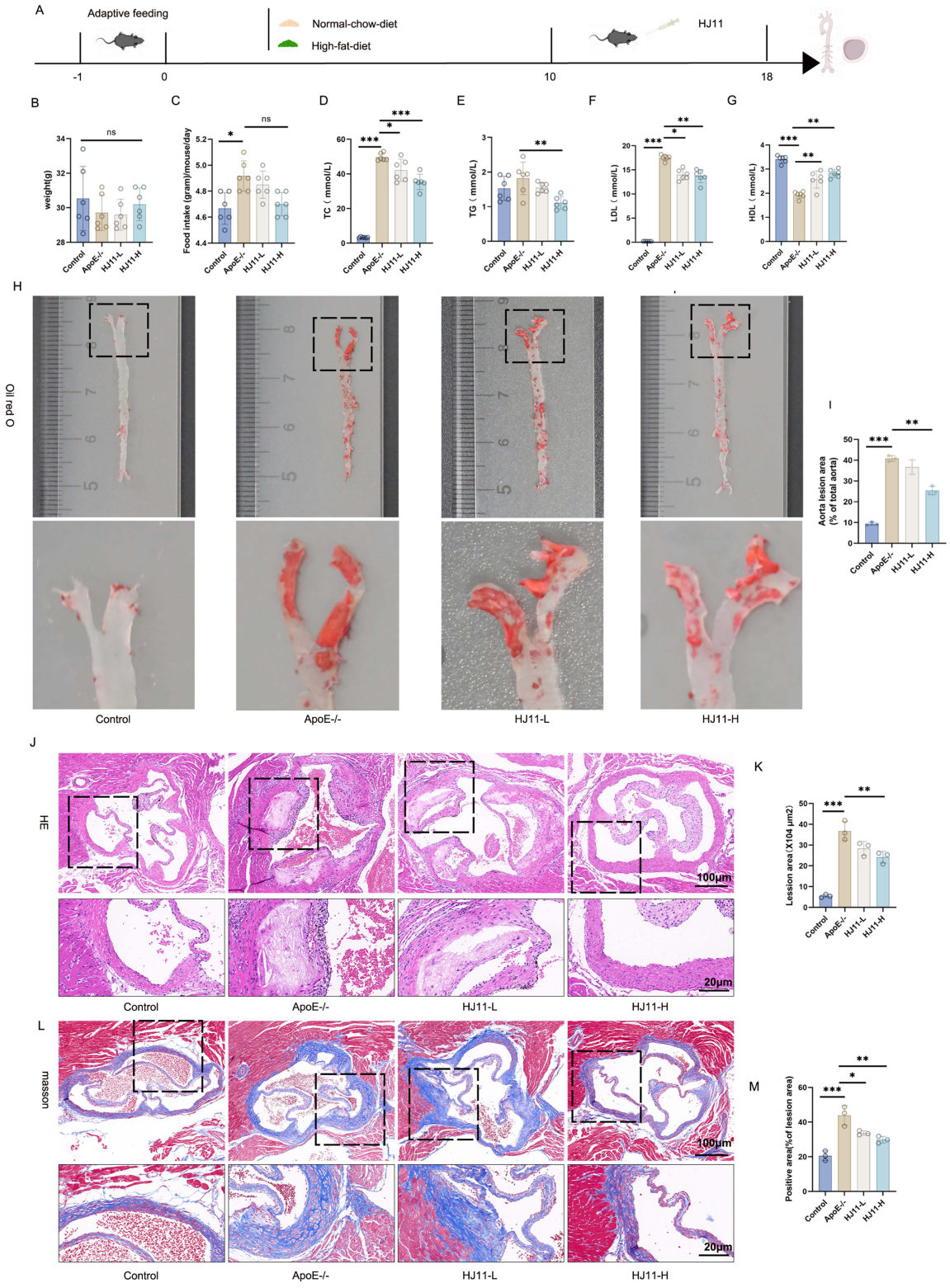

Figure 1 HJ11 formula inhibited the formation of atherosclerotic plaque in high-fat diet-induced atherosclerosis in ApoE−/− mice. (**A**) The experimental flow chart of animal study. (**B**) Body weights of mice were measured at the end of the experiment. (**C**) The food intake of mice was monitored at the end of the experiment. (**D**–**G**) At the end of the experiment, the serum levels of TC, TG, LDL and HDL in mice were detected by biochemistry test. (**H** and **I**) To appraise atherosclerosis, Oil Red O staining of the entire aorta of mice was carried out. The squares indicate the aortic arch region, shown magnified below to better visualize the atherosclerotic lesions. (**J** and **K**) Vascular pathology of the aorta was detected by HE staining.The squares indicate the regions with the most severe vascular lesions, which are shown magnified below to better visualize the histopathological changes. (**L** and **M**) Masson staining was adopted on the aorta to appraise the collagen deposition.The squares indicate the regions with the most pronounced vascular lesions and collagen deposition, shown magnified to better visualize the histopathological changes. **P* < 0.05. ***P* < 0.01. ****P* < 0.001. The symbol of "ns" meant a difference that was not statistically significant.

https://doi.org/10.2147/JIR.S523304

To appraise the influence of HJ11 formula on atherosclerosis, the entire aorta of each mouse was gathered for Oil Red O staining. The enlarged aorta lesion area was presented in ApoE−/− mice of the ApoE−/− group, when relative to C57BL/6J mice of the Control group ($P < 0.001$). A high dose of the HJ11 formula significantly reduced the aortic lesion area compared to the ApoE−/− group ($P < 0.01$). (Figure 1H and I). Vascular pathology and collagen deposition of the aorta were evaluated by HE staining and Masson staining, respectively. The extended lesion area and collagen deposition area occurred in ApoE−/− mice of the ApoE−/− group, when matched to the Control group ($P < 0.001$). A low dose of HJ11 formula reduced the collagen deposition area (rather than lesion area) in ApoE−/− mice ($P < 0.05$). HJ11 formula at a high dose effectively diminished lesion area and collagen deposition area in ApoE−/− mice ($P < 0.01$) (Figure 1J–L and M). The findings herein showed that HJ11 formula hindered the formation of atherosclerotic plaque.

HJ11 Formula Attenuated the Inflammation of Endothelial Cells and Macrophages, the Proliferation of VSMC, and Inactivated the TLR4/NF-κB P65 Pathway in High-Fat Diet-Induced Atherosclerosis in ApoE−/− Mice

The changes in serum cytokines was tested by ELISA, including LPS, IL-6, IL-1β, VCAM-1, TNF-α, and MMP-9. As a result, ApoE−/− mice of the ApoE−/− group showed a distinct elevation in these serum cytokines, when compared to the Control group ($P < 0.01$ or $P < 0.001$). By contrast, HJ11 formula at a low dose led to a reduction in serum LPS, IL-6, VCAM-1, and MMP-9 levels ($P < 0.05$), while a high dose of HJ11 formula reduced the levels of serum LPS, IL-6, VCAM-1, and MMP-9 ($P < 0.05$ or $P < 0.01$) (Figure 2A–F).

Immunohistochemistry of the aortic root was performed to assess TLR4 expression. Compared to the minimal TLR4 expression observed in the control group, ApoE−/− mice exhibited significantly elevated TLR4 levels in the aortic root ($P < 0.001$). Treatment with the HJ11 formula, at both low and high doses, significantly reduced TLR4 expression ($P < 0.05$ or $P < 0.01$) (Figure 2G and H). To evaluate macrophage and endothelial inflammation as well as vascular smooth muscle cell (VSMC) proliferation, immunofluorescence staining of the aortic root was conducted. ApoE−/− mice displayed markedly increased expression of α-SMA/CD68 and p-p65/CD31 compared to controls ($P < 0.05$ or $P < 0.01$) (Figure 2I–L). Furthermore, mRNA levels of NF-κB p65 and TLR4 in the aortic root were measured by qRT-PCR. ApoE−/− mice showed significantly higher expression of both genes compared to the control group ($P < 0.01$ or $P < 0.001$), while high-dose HJ11 treatment significantly downregulated their expression ($P < 0.01$) (Figure 2M and N). Collectively, these findings indicate that HJ11 formula alleviates endothelial and macrophage inflammation, suppresses VSMC proliferation, and inactivates the TLR4/NF-κB p65 signaling pathway in atherosclerosis.

HJ11 Formula Relieved the Compromised Intestinal Barrier in High-Fat Diet-Induced Atherosclerosis in ApoE−/− Mice

To research the function of HJ11 formula on the intestine in atherosclerosis, this work performed HE staining with the intestine of mice in each group. C57BL/6J mice of the Control group were with the intact intestinal structure, normal chorionic glands, as well as intact submucosa and lamina propria. However, the severely disrupted intestinal structure was discovered in ApoE−/− mice, such as the damaged structure of intestinal mucosa and mucosal epithelium, the destroyed crypt-villus, severe inflammatory cell infiltration and epithelial damage. In contrast, these intestinal damage phenomena were relieved in ApoE−/− mice of the two HJ11 formula induction groups (the HJ11-L group and the HJ11-H group), especially the HJ11-H group (Figure 3A).

Alcian blue staining (Figure 3B) and immunofluorescence staining (Figure 3C) of the intestine showed the remarkably reduced goblet cells and ZO-1 expression in ApoE−/− mice, when matched to the Control group ($P < 0.01$). Intriguingly, a high dose of HJ11 formula prominently increased the number of goblet cells as well as the expression of ZO-1, in comparison to the ApoE−/− group (Figure 3D and E) ($P < 0.05$).

LPS level in the intestine and FITC-Dextran level in the serum were explored to research the intestinal inflammation and the intestinal permeability. In contrast to the Control group, higher LPS and FITC-Dextran levels were monitored in ApoE−/− mice ($P < 0.01$). Conversely, ApoE−/− mice of the two HJ11 formula induction groups (the HJ11-L group and

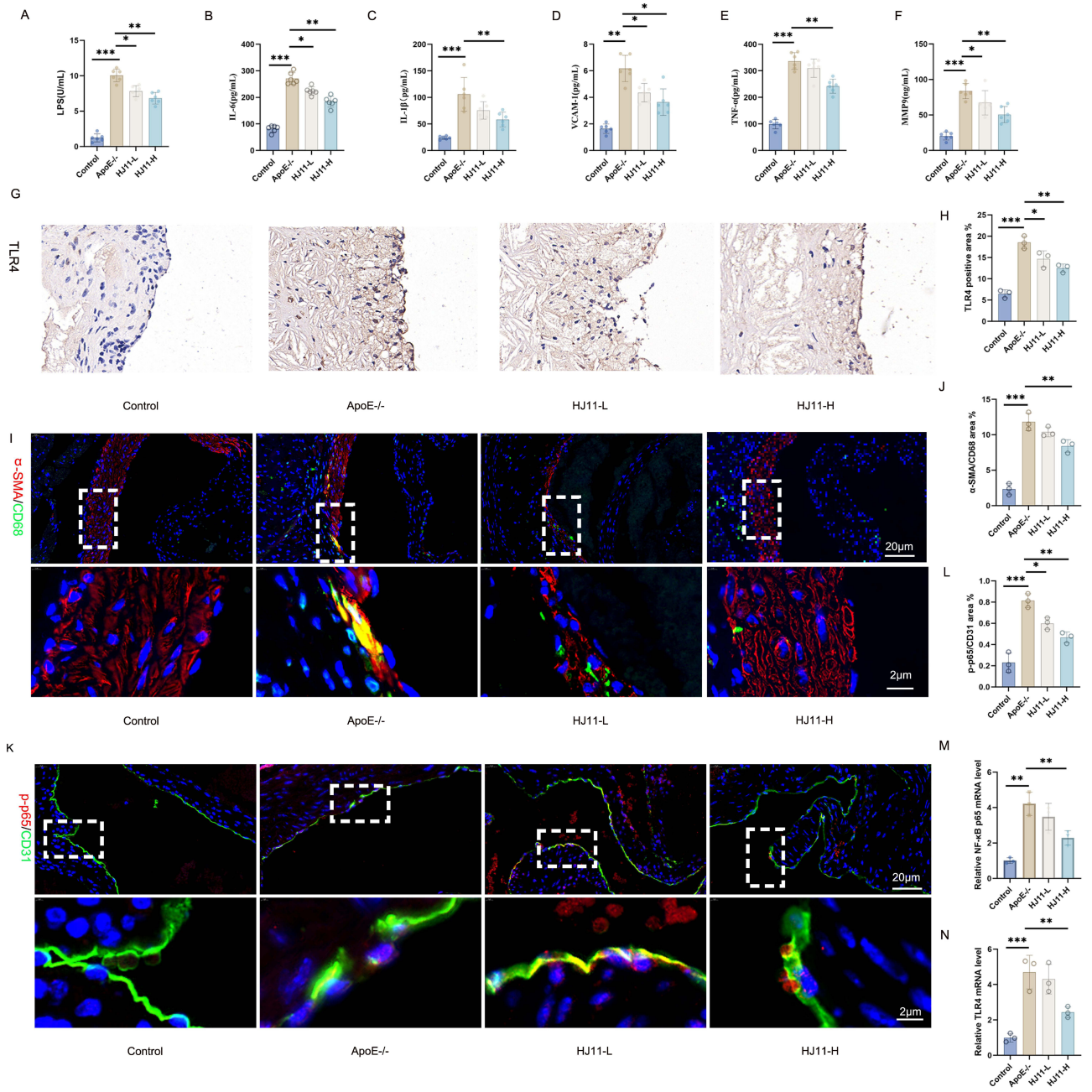

Figure 2 HJ11 formula attenuated the inflammation of endothelial cells and macrophages, the proliferation of VSMC, and inactivated the TLR4/NF-κB P65 pathway in high-fat diet-induced atherosclerosis in ApoE−/− mice. (**A**–**F**) Serum levels of IL-6, IL-1β, VCAM-1, TNF-α, MMP-9, and LPS in mice were measured by ELISA. (**G** and **H**) Immunohistochemistry was used to evaluate TLR4 expression in the aortic root of mice. (**I**–**K**) Immunofluorescence staining of the aortic root was performed to assess endothelial and macrophage inflammation (p-p65/CD31, α-SMA/CD68) and VSMC proliferation. The dotted rectangles indicate representative lesion or endothelial regions selected for higher magnification to better visualize marker expression and colocalization. (**L**–**N**) The mRNA expression of p-p65, NF-κB p65, and TLR4 in the aortic root of mice was determined by qRT-PCR.*$P < 0.05$. **$P < 0.01$. ***$P < 0.001$.

the HJ11-H group) exhibited a much reduction in the levels of LPS and FITC-Dextran, in comparison to the ApoE−/− group ($P < 0.05$) (Figure 3F and G).

qRT-PCR of the intestine showed the lowly expressed mRNAs for Occludin, ZO-1 and Claudin-3 in ApoE−/− mice, when referring to the Control group ($P < 0.01$ or $P < 0.001$). A high dose of HJ11 formula induced a significant elevation in the expression of mRNAs for Occludin, ZO-1 and Claudin-3, comparatively ($P < 0.05$) (Figure S2).

TEM was executed to microscopically observe the damage of the intestine in mice of each group. C57BL/6J mice of the Control group presented the regularly arranged intestinal epithelial cells, the closely and regularly arranged

https://doi.org/10.2147/JIR.S523304

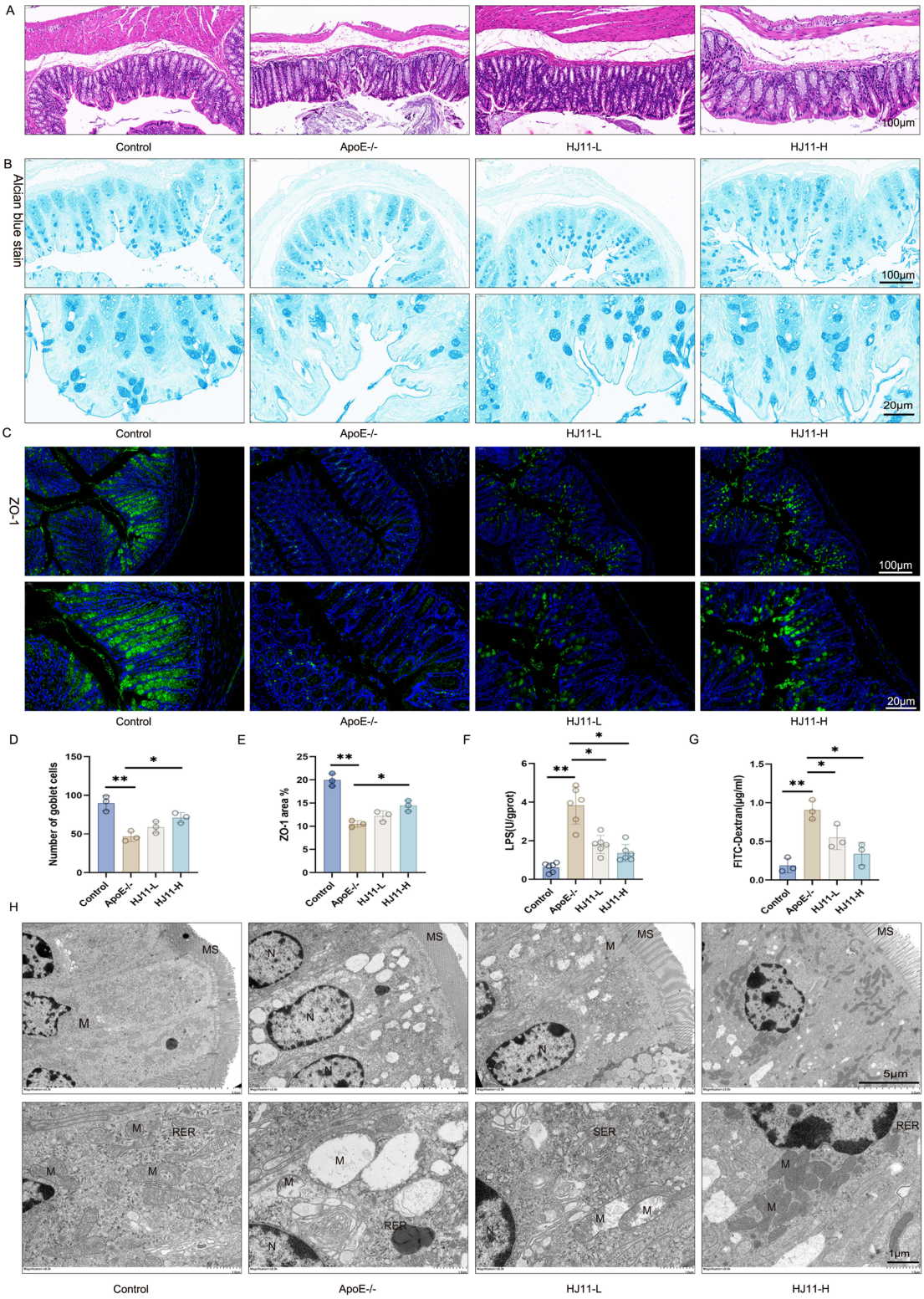

Figure 3 HJ11 formula mitigated the damaged intestinal barrier in high-fat diet-induced atherosclerosis in ApoE−/− mice. (**A**) HE staining of the intestine was executed to explore the intestinal damage. (**B**) Alcian blue staining of the intestine was utilized to investigate the number of goblet cells. (**C**) Immunofluorescence staining for ZO-1 was performed in the intestine to assess intestinal permeability. (**D**) Quantitative analysis of goblet cell numbers based on Alcian blue staining shown in (**B**). (**E**) Quantitative analysis of ZO-1 expression based on immunofluorescence staining shown in (**C**). (**F**) LPS change in the intestine was tested by ELISA to evaluate intestinal inflammation. (**G**) The serum FITC-Dextran level was detected to evaluate intestinal permeability. (**H**) TEM was executed to microscopically observe the damage of the intestine. *$P < 0.05$. **$P < 0.01$.

Abbreviations: M, mitochondria; MS, microvilli; LJ, intestinal epithelial cell junctions; RER, rough endoplasmic reticulum; N, nuclei; SER, smooth endoplasmic reticulum.

microvilli, the abundantly and structurally intact mitochondria and rough endoplasmic reticulum, as well as the tight epithelial cell junctions. Unfortunately, in ApoE−/− mice, the severe damage of the intestine was observed, such as the swollen intestinal epithelial cells, the irregularly shaped nuclei, the highly swollen mitochondria, the reduced rough endoplasmic reticulum, hyperplasia of smooth endoplasmic reticulum, as well as structurally disorganized epithelial cell junctions. Compared to the ApoE−/−group, these intestinal injuries were significantly alleviated in both HJ11-treated groups (the HJ11-L group and the HJ11-H group) (Figure 3H). Taken together, HJ11 formula could effectively mitigated the damaged intestinal barrier in atherosclerosis.

HJ11 Formula Improved the Microbiological Disorders of the Intestinal Flora in High-Fat Diet-Induced Atherosclerosis in ApoE−/− Mice

To research the effect of HJ11 formula on the intestinal microbes in atherosclerosis, 16S rDNA sequencing of the v3+ v4 region was performed on the faeces of mice (including the Control group, the ApoE−/− group and the HJ11-H group). The number of OTUs shared by different groups was visualized by Venn diagram (Figure 4A). Chao1 index has the ability to evaluate the species richness. ApoE−/− mice displayed a much lower Chao1 index than that of the Control group ($P < 0.001$). However, the difference in Chao1 index was not significant between the ApoE−/− group and the HJ11-H group (Figure 4B). Simpson index, a measure of the community "evenness", is ranged from 0 to 1. A Simpson index closer to 1 indicates a more homogeneous distribution of taxa. A similar Simpson index was found in the faeces of mice in the three groups, indicating a similar microbial distribution in the intestine of mice in the three groups (Figure 4C). Shannon index is a diversity index, which takes into account the number of individuals and taxa. A much reduction in Shannon index was obtained in the faeces of ApoE−/− mice in the ApoE−/− group, when referred to the Control group ($P < 0.01$). Oppositely, a high dose of HJ11 formula treatment led to an increase in Shannon index in ApoE−/− (the HJ11-H group vs the ApoE−/− group) ($P < 0.05$) (Figure 4D). Followed by this, this work analyzed the abundance of intestinal microbes at levels of Phylum, Class, Order, Family and Genus. The top 10 intestinal microbes in terms of abundance were shown in Figure 4E–I, classified according to Phylum, Class, Order, Family and Genus. In ApoE−/−mice with atherosclerosis, HJ11 formula treatment increased Verrucomicrobia abundance at PhylApoE−/− m level. At Class level, it elevated Actinobacteria abundance, and diminished the abundance of Clostridia and Coriobacteriia. Besides, it reduced the abundance of Clostridiales and Coriobacteriales, and promoted the abundance of Verrucomicrobiales and Bifidobacterialles at Order level. In terms of Family level, it reduced S24-7, Ruminococcaceae and Coriobacteriaceae abundance, and increased Verrucomicrobiaceae and Bacteroidaceae abundance. Moreover, at Genus level, it increased Akkermansia, Bacteroides, Bifidobacterium abundance, and reduced the abundance of Ruminococcus and Oscillospira. Thus, it could be noticed that HJ11 formula affected the α-diversity and taxonomic diversity of intestinal microbes in mice with atherosclerosis. In ApoE−/− mice with atherosclerosis, the differential metabolic pathways induced by HJ11 formula treatment were shown (the ApoE−/− group vs the HJ11-H group) (Figure 4J).

Moreover, by the LEfSe method, this work identified the high-dimensional biomarkers in the intestinal microbiota of ApoE−/− mice. The LDA threshold was set to 2.6, and the taxa with LDA scores more than 2.6 were regarded as the important biomarkers (Figure 4K). Therefore, all of these above data suggested that the change of intestinal microbiota was involved in the development of atherosclerosis. HJ11 formula could improve the diversity of intestinal microbiota in ApoE−/− mice with atherosclerosis.

HJ11 Formula Regulated the Fecal Metabolites in High-Fat Diet-Induced Atherosclerosis in ApoE−/− Mice

This work studied the effect of HJ11 formula on the metabolites in ApoE−/− mice with atherosclerosis. The differential metabolites among the three groups (the Control group, the

ApoE−/− group, as well as the HJ11-H group) were shown by Venn diagram (Figure 5A) and Upset Venn Diagram (Figure 5B). OPLS-DA was employed to distinguish the differential metabolites. It showed a more clustered samples within group, but obviously dispersed samples between two groups (Figure 5C). Subsequently, these differential metabolites in the faeces of mice among the Control group, the ApoE−/− group, and the HJ11-L group were detected through the LC-MS. As comparison to C57BL/6J mice of the Control group, ApoE−/− mice of the ApoE−/− group showed higher 2-Methoxyestrone, but

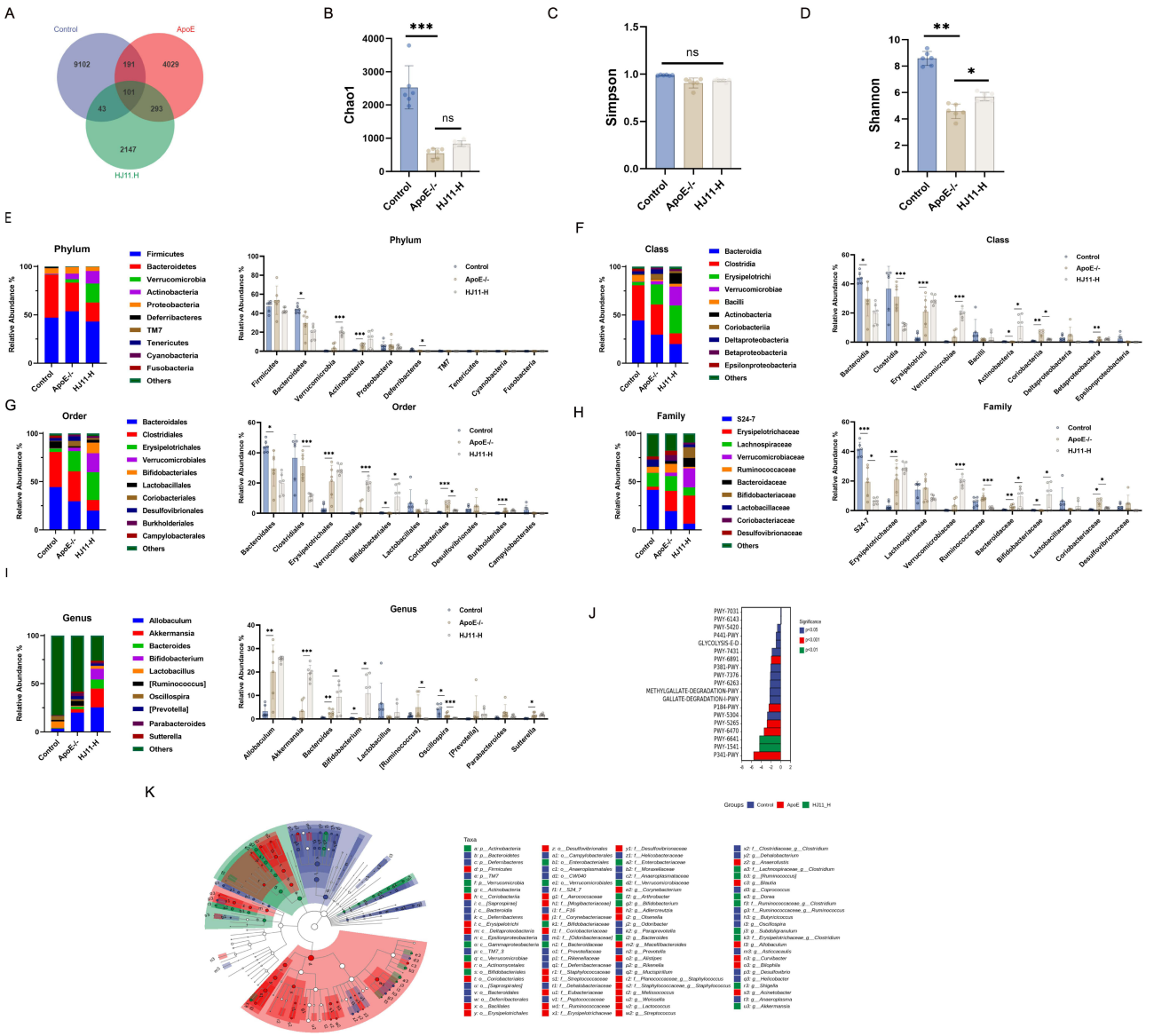

Figure 4 HJ11 formula improved the microbiological disorders of the intestinal flora in high-fat diet-induced atherosclerosis in ApoE−/− mice. (**A**) The OTUs in the faeces of mice was presented by the form of Venn diagram. (**B**–**D**) The diversity of intestinal microbes in mice was evaluated by Chao1 index, Simpson index and Shannon index. (**E-I**) The taxonomic diversity of intestinal microbes in mice was appraised at the Phylum, Class, Order, Family and Genus levels. (**J**) The differential metabolic pathways in mice with atherosclerosis induced by HJ11 formula treatment were analyzed by the metagenomeSeq method with R language software. (**K**) The LEfSe analysis was implemented on the intestinal microbiota in mice. *$P < 0.05$. **$P < 0.01$. ***$P < 0.001$. The symbol of "ns" meant a difference that was not statistically significant.

lower trans-Cinnamate, L-Arginine, Methyl beta-D-galactoside, D-Ribose 5-phosphate, 13-Dihydro-(2H)-indol-2-one, Acetylcholine, gamma-L-Glutamyl-L-2-aminobutyrate, Dhurrin, D-Xylose, 5-Methoxyindoleacetate and 4-Acetamidobutanoate ($P < 0.05$, $P < 0.01$ or $P < 0.001$). Simultaneously, in contrast to the ApoE−/− group, higher 2-Methoxyestrone, D-Ribose 5-phosphate, Methyl(indol-3-yl)acetate, gamma-L-Glutamyl-L-2-aminobutyrate, 5-Methoxyindoleacetate and 4-Acetamidobutanoate were discovered in the HJ11-L group ($P < 0.05$ or $P < 0.001$) (Figure 5D). The differential metabolites and the differential flora in the faeces of mice among the Control group, the ApoE −/− group, and the HJ11-L group were analyzed. Differential metabolites included trans-Cinnamate, L-Arginine, Methyl beta-D-galactodise, D-Ribose 5-phosphate, 1,3-Dihydro-(2H)-indol-2one, Acetylcholine, gamma-L-Glutamyl-L-2-aminobutyrate, Dhurrin, D-Xylose, gamma-Glutamylcysteine, o-Cresol, and Cholesterol sulfate (Figure 5E). Differential flora included Coriobacteriia, Coriobacteriales, and Coriobacteriaceae (Figure 5F). All of these data implied that HJ11 formula affected the fecal metabolites in atherosclerosis ApoE−/− mice that induced by high-fat diet.

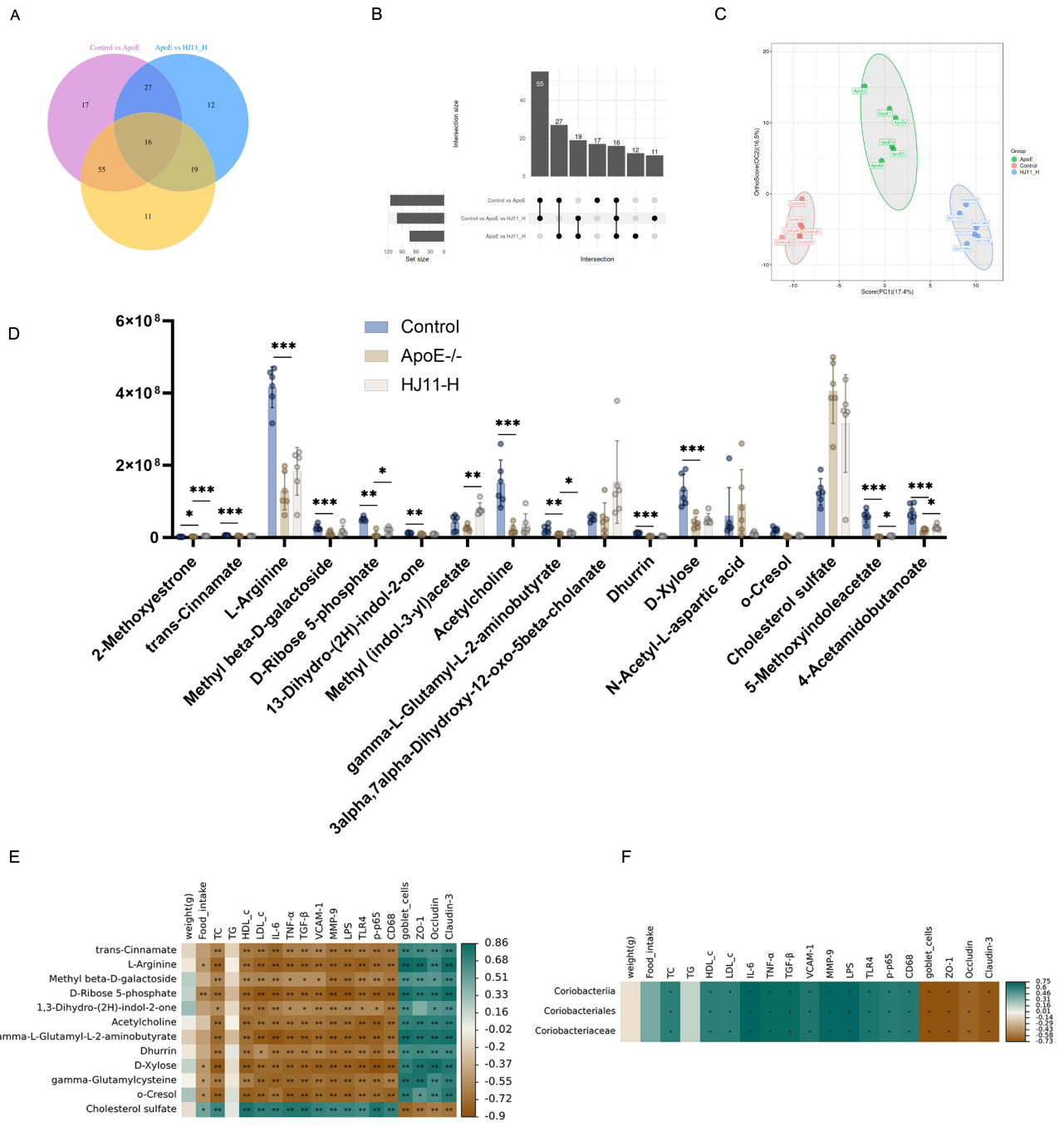

Figure 5 HJ11 formula regulated the fecal metabolites in high-fat diet-induced atherosclerosis in ApoE−/− mice. (**A** and **B**) Venn diagram and Upset Venn diagram were prepared to display the number of fecal metabolites in mice of the Control group, the ApoE−/− group, and the HJ11-L group. (**C**) OPLS-DA was performed to distinguish the differential metabolites among the Control group, the ApoE−/− group, and the HJ11-L group. (**D**) The levels of the differential metabolites among the Control group, the ApoE−/− group, and the HJ11-L group were analyzed by LC-MS analysis. (**E** and **F**) The differential metabolites and the differential flora in the faeces of mice among the Control group, the ApoE−/− group, and the HJ11-L group were listed. *$P < 0.05$. **$P < 0.01$. ***$P < 0.001$.

HJ11 Formula Might Enhance the Proliferation and Migration, and Suppress the Inflammation Response of the LPS-Induced Mouse Aortic Vascular Endothelial Cells by Inactivating the TLR4/MYD88/IκB-α Pathway

Atherosclerosis is a chronic inflammatory disease involving blood vessels. Thus, this study induced mouse aortic vascular endothelial cells with LPS to establish the cell model of atherosclerosis. As shown in Figure 6A, LPS treatment (the LPS group) induced a significant reduction in the proliferation ability of mouse aortic vascular endothelial cells, as relative to the Control

https://doi.org/10.2147/JIR.S523304

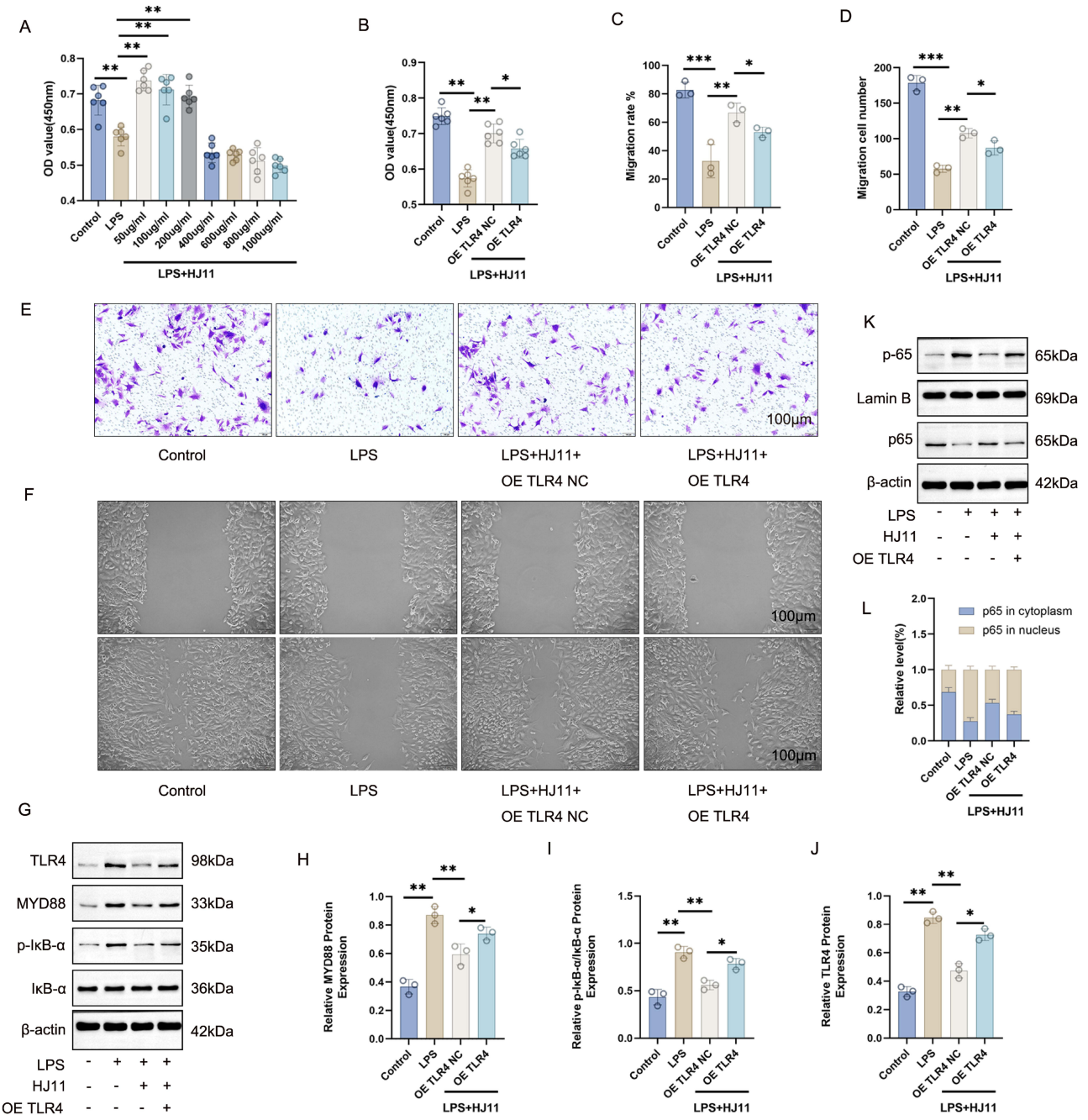

Figure 6 HJ11 formula might enhance the proliferation and migration, and suppress the inflammation response of the LPS-induced mouse aortic vascular endothelial cells by inactivating the TLR4/MYD88/IκB-α pathway. (**A**) CCK-8 assay was performed to determine the safe and effective concentration of HJ11 formula on the LPS-induced mouse aortic vascular endothelial cells. (**B**) The proliferation ability of mouse aortic vascular endothelial cells in each group was researched by CCK-8 assay. (**C**–**F**) CCK-8 assay, Transwell experiment, and cell scratch experiment were utilized to research the proliferation and migration abilities of mouse aortic vascular endothelial cells. (**G**–**J**) Western blotting was applied to research the activity of the TLR4/MYD88/IκB-α pathway in mouse aortic vascular endothelial cells of each group. (**K** and **L**) The entry of p65 protein in mouse aortic vascular endothelial cells was evaluated by Western blotting. *$P < 0.05$. **$P < 0.01$. ***$P < 0.001$.

group ($P < 0.01$). However, HJ11 formula at concentrations of 50, 100 and 200 μg/mL markedly increased the proliferation ability of the LPS-induced mouse aortic vascular endothelial cells ($P < 0.01$). It should be noted that, the LPS-induced mouse aortic vascular endothelial cells that treated by 50 μg/mL HJ11 formula had higher proliferation ability than those treated by 100 and 200 μg/mL HJ11 formula. Thus, HJ11 formula at a concentration of 50 μg/mL was selected in the following experiment.

To research whether HJ11 formula relieved atherosclerosis by regulating the TLR4/MYD88/IκB-α pathway, mouse aortic vascular endothelial cells were transfected by TLR4 overexpression vectors (or negative expression vectors) and

then treated with LPS and HJ11 formula (50 μg/mL). As exhibited in Figure 6B–F, mouse aortic vascular endothelial cells of the LPS group possessed distinctly lower proliferation and migration abilities, as referring to those of the Control group ($P < 0.01$ or $P < 0.001$). In contrast to the LPS group, the LPS + HJ11 + OE TLR4 NC group displayed higher proliferation and migration abilities ($P < 0.01$). Conversely, when matched to the LPS + HJ11 + OE TLR4 NC group, the proliferation and migration abilities of mouse aortic vascular endothelial cells was remarkably decreased in the LPS + HJ11 + OE TLR4 group ($P < 0.05$). Thus, TLR4 up-regulation abolished the promotion of HJ11 formula on the proliferation and migration abilities of the LPS-induced mouse aortic vascular endothelial cells.

To research the activity of the TLR4/MYD88/IκB-α pathway, Western blotting was implemented to detect the expression of TLR4, MYD88 and p-IκB-α/IκB-α. The results were shown in Figure 6G–J. LPS induction (the LPS group) induced a distinctly up-regulation of proteins for TLR4, MYD88 and p-IκB-α/IκB-α in mouse aortic vascular endothelial cells, as referred to the Control group ($P < 0.01$). In comparison to the LPS group, the expression of proteins for TLR4, MYD88 and p-IκB-α/IκB-α was markedly down-regulated in mouse aortic vascular endothelial cells of the LPS + HJ11 + OE TLR4 NC group ($P < 0.01$). Oppositely, when matched to the LPS + HJ11 + OE TLR4 NC group, the level of proteins for TLR4, MYD88 and p-IκB-α/IκB-αt was pronouncedly increased in mouse aortic vascular endothelial cells of the LPS + HJ11 + OE TLR4 group ($P < 0.05$).

As we know, the entry of p65 protein is involved in the regulation of inflammation. Thus, this study investigated the effect of HJ11 formula on the entry of p65 protein into the nucleus by Western blotting (Figure 6K and L). By referring to the Control group, LPS induction (the LPS group) facilitated the p65 protein entry into the nucleus in mouse aortic vascular endothelial cells. However, the entry of p65 protein into the nucleus was much attenuated in mouse aortic vascular endothelial cells of the LPS + HJ11 + OE TLR4 NC group, as relative to the LPS group. In contrast to the LPS + HJ11 + OE TLR4 NC group, mouse aortic vascular endothelial cells of the LPS + HJ11 + OE TLR4 group showed the intensified p65 protein entry into the nucleus. Taken together, HJ11 formula enhanced proliferation and migration, and suppressed the inflammation response of the LPS-induced mouse aortic vascular endothelial cells, possibly by inactivating the TLR4/MYD88/IκB-α pathway.

Discussion

This study demonstrates that the Chinese medicine formula HJ11 alleviates atherosclerotic injury through multi-target mechanisms involving lipid regulation, anti-inflammatory effects, and modulation of the heart–gut axis. In ApoE−/− mice, HJ11 reduced serum TC, TG, and LDL while increasing HDL, inhibited aortic plaque formation and collagen deposition, alleviated endothelial and macrophage inflammation, suppressed VSMC proliferation, and downregulated pro-inflammatory cytokines (IL-6, TNF-α, LPS). This finding is consistent with the well-established role of dyslipidemia—particularly elevated LDL and reduced HDL—as a major contributor to atherosclerosis progression.[24,25] It also improved intestinal barrier function by enhancing ZO-1 and Occludin expression, increasing goblet cell counts, and restoring microbiota balance (for example, increasing Akkermansia). Mechanistically, these effects were mediated via inactivation of the TLR4/MYD88/IκB-α pathway, as confirmed in vitro, and were abolished by TLR4 overexpression. Notably, HJ11 also reduces serum MMP-9 levels and collagen deposition, both of which are critical determinants of plaque stability.[26] These findings are novel in establishing a mechanistic link between HJ11 and the heart–gut axis, highlighting its promise as a multi-modal therapeutic candidate for atherosclerosis and related cardiovascular diseases.

In addition, HJ11 exerts anti-inflammatory effects by targeting multiple cell types and signaling pathways. Our results show that HJ11 downregulates pro-inflammatory cytokines (IL-6, TNF-α, and LPS), alleviates inflammation in endothelial cells and macrophages,[27–32] and suppresses vascular smooth muscle cell (VSMC) proliferation. Inflammation—particularly macrophage-mediated and endothelial-driven responses—is a central pathological process that accelerates atherosclerosis. Mechanistically, HJ11 reduces the expression of p-p65/CD31 (a marker of endothelial inflammation) and α-SMA/CD68 (markers of VSMC proliferation and macrophage infiltration) in the aortic root. It also inactivates the TLR4/NF-κB p65 signaling pathway, a well-established driver of atherosclerotic inflammation.[33,34] These findings extend previous reports of HJ11's anti-inflammatory effects in acute cardiovascular injury to chronic atherosclerotic disease.[11,12]

Beyond inflammation, HJ11 also modulates the heart-gut axis to alleviate systemic inflammation. Our results indicate that HJ11 enhances intestinal barrier function by upregulating the expression of tight junction proteins (ZO-1 and Occludin) and increasing goblet cell numbers, thereby reducing intestinal permeability and circulating LPS levels. In parallel, 16S rDNA

sequencing reveals that HJ11 promotes gut microbial homeostasis—such as increasing the abundance of Akkermansia—and improves fecal metabolite profiles. These findings align with the emerging paradigm that intestinal barrier dysfunction and microbial dysbiosis contribute to atherosclerosis by facilitating LPS translocation and systemic inflammation,[35,36] supporting the clinical relevance of HJ11's regulatory effects on the heart-gut axis.

In vitro assays in LPS-stimulated mouse aortic vascular endothelial cells demonstrate that HJ11 promotes cell proliferation and migration by inactivating the TLR4/MYD88/IκB-α signaling pathway, an effect abolished by TLR4 overexpression. This aligns with previous studies showing that targeting the TLR4 pathway can alleviate atherosclerotic inflammation,[20,37] links HJ11's therapeutic effect to this specific molecular mechanism. Our earlier work demonstrated that HJ11 ameliorates atherosclerosis by downregulating pro-inflammatory cytokines and targeting AKT1.[38] The present study builds upon previous findings by further associating HJ11 with modulation of the heart-gut axis. We demonstrate that HJ11 regulates gut microbiota composition and enhances intestinal barrier integrity, thereby reducing LPS translocation. Furthermore, we provide direct mechanistic evidence that the TLR4/MYD88/IκB-α signaling pathway is a key mediator of HJ11's anti-inflammatory effects, as confirmed through TLR4 overexpression assays. These findings clarify the signaling cascade underlying HJ11's protective role in atherosclerosis.

Notably, HJ11 modulates the TLR4 signaling pathway indirectly by regulating the gut microbiota. In this study, HJ11 significantly increases the abundance of beneficial bacteria such as Akkermansia, reduces the proportion of pro-inflammatory taxa, and lowers intestinal LPS release (Figures 3 and 4). These changes contribute to improved intestinal barrier integrity—evidenced by increased goblet cells and elevated expression of tight junction proteins (ZO-1 and Occludin)—and ultimately reduce TLR4 pathway activation. Together, these findings support the existence of a "microbiota–barrier–LPS–TLR4" regulatory axis through which HJ11 alleviates systemic inflammation.

Supporting this concept, a previous study reported that NG-R1, a bioactive compound from Panax notoginseng, reduced intestinal permeability and serum LPS levels in a middle cerebral artery occlusion/reperfusion (MCAO/R) model by restoring the gut microbiota balance—specifically, by reversing the enrichment of Proteobacteria and depletion of Bacteroidota—thereby suppressing TLR4 signaling.[39] These independent findings further validate the role of gut microbiota and intestinal barrier function in regulating TLR4-mediated inflammation and suggest that this may be a general mechanism through which Chinese herbal compounds exert protective effects.

This study has several limitations that should be acknowledged. First, the animal model used (ApoE−/− mice fed a high-fat diet) reproduces key features of human atherosclerosis but does not fully capture the complexity of the human disease. Second, the dosing regimen of HJ11 (6.63 g/kg and 13.26 g/kg) was based on clinical dose conversion, but the optimal dosage, frequency, and duration of administration in humans remain to be determined. Third, the study lacks a germ-free or antibiotic-treated mouse group, which limits mechanistic insightsinto the causal role of gut microbiota. Moreover, due to time and resource constraints, we wereunable to further verify the specific contribution of high-fat diet–induced microbiota alterations to atherosclerosis progression, which represents another limitation. Finally, differences between human and murine gut microbiota and immune responses may affect the translational relevanceof our findings, and further validation in clinical studies is necessary.

Conclusion

This study demonstrates that HJ11 attenuates atherosclerotic injury by modulating the inflammatory response along the heart-gut axis. The HJ11 formula inhibits plaque formation and vascular inflammation, restores intestinal barrier integrity, and improves gut microbiota composition and metabolite profiles in ApoE−/− mice. Its therapeutic effects may be mediated through inactivation of the TLR4/MYD88/IκB-α signaling pathway in a microbiota-dependent manner. These findings provide experimental evidence supporting the clinical potential of HJ11 in treating coronary heart disease and underscore the promise of targeting the heart-gut axis and TLR4 signaling as novel strategies for atherosclerosis therapy.

Abbreviations

α-SMA, α-smooth muscle actin; CCK-8, Cell counting kit-8; DAPI, 4′, 6-diamidino-2-phenylindole; ECM, Endothelial Cell Medium; ELISA, Enzyme-linked immunosorbent assay; FBS, Fetal bovine serum; FITC, Fluorescein isothiocyanate; HDL, High-density lipoprotein; HE, Hematoxylin and eosin; IκB-α, IkappaB-α; IL-1β, Interleukin-1β; IL-6,

Interleukin-6; LC-MS, Liquid chromatography-mass spectrometry; LEfSe, Line discriminant analysis effect size; LDA, Line discriminant analysis; LDL, Low-density lipoprotein; LPS, Lipopolysaccharide; MMP-9, Matrix metalloproteinase-9; MYD88, Myeloid differentiation factor-88; NF-κB, Nuclear factor-kappaB; OD, Optical density; OPLS-DA, Orthogonal Projections to Latent Structures Discriminant Analysis; OTUs, Operational taxonomic units; p-65, phosphorylated p65; p-IκB-α, Phosphorylated IkappaB-α; PVDF, Polyvinylidene fluoride; qRT-PCR, Real-time quantitative reverse transcription-polymerase chain reaction; TC, Total cholesterol; TEM, Transmission electron microscopy; TG, Triglycerides; TLR4, Toll-like receptor 4; TNF-α, Tumor necrosis factor-α; VCAM-1, Vascular cellular adhesion molecule-1; VSMC, vascular smooth muscle cells;ZO-1, Zonulaoeeludens-1.

Data Sharing Statement

The data that support the findings of this study are available from Fangyuan Zhang (zhangfangyuan@ucas.ac.cn) upon reasonable request.

Author Contributions

All authors made a significant contribution to the work reported, whether that is in the conception, study design, execution, acquisition of data, analysis and interpretation, or in all these areas; took part in drafting, revising or critically reviewing the article; gave final approval of the version to be published; have agreed on the journal to which the article has been submitted; and agree to be accountable for all aspects of the work.

Funding

This work was supported by grants from the National Key research and Development Program of China (NO.2019YFC1708501); National Natural Science Foundation of China (NO.82074316); China Postdoctoral Science Foundation (NO.2024M760703).

Disclosure

The authors declare that they have no known competing financial interests or personal relationships that could have appeared to influence the work reported in this paper.

References

1. Khan AW, Paneni F, Jandeleit-Dahm KAM. Cell-specific epigenetic changes in atherosclerosis. *Clin Sci*. 2021;135(9):1165–1187. doi:10.1042/cs20201066
2. Bentzon JF, Otsuka F, Virmani R, Falk E. Mechanisms of plaque formation and rupture. *Circul Res*. 2014;114(12):1852. doi:10.1161/CIRCRESAHA.114.302721
3. Vergallo R, Crea F. *Atherosclerotic Plaque Disruption and Healing*. Oxford University Press; 2020.
4. Sui D, Yu H. Protective roles of apremilast via Sirtuin 1 in atherosclerosis. *Bioengineered*. 2022;13(5):13872–13881. doi:10.1080/21655979.2022.2085390
5. Verhaar BJ, Prodan A, Nieuwdorp M, Muller M. Gut microbiota in hypertension and atherosclerosis: a review. *Nutrients*. 2020;12(10):2982. doi:10.3390/nu12102982
6. Puylaert P, Zurek M, Rayner KJ, De Meyer GR, Martinet W. Regulated necrosis in atherosclerosis. *Arteriosclerosis Thrombosis Vasc Biol*. 2022;42(11):1283–1306. doi:10.1161/ATVBAHA.122.318177
7. Liu H, Zhu L, Chen L, Li L. Therapeutic potential of traditional Chinese medicine in atherosclerosis: a review. *Phytother Res*. 2022;36(11):4080–4100. doi:10.1002/ptr.7590
8. Liao M, Xie Q, Zhao Y, et al. Main active components of Si-Miao-Yong-An decoction (SMYAD) attenuate autophagy and apoptosis via the PDE5A-AKT and TLR4-NOX4 pathways in isoproterenol (ISO)-induced heart failure models. *Pharmacol Res*. 2022;176:106077. doi:10.1016/j.phrs.2022.106077
9. Chen X, Ge Q, Zhao Y, Guo X, Zhang J. Effect of Si-Miao-Yong-An decoction on the differentiation of monocytes, macrophages, and regulatory T cells in ApoE-/-mice. *J Ethnopharmacol*. 2021;276:114178. doi:10.1016/j.jep.2021.114178
10. Qi Z, Yan Z, Zhu K, et al. Novel treatment from a botanical formulation Si-Miao-Yong-an decoction inhibits vasa vasorum angiogenesis and stabilizes atherosclerosis plaques via the Wnt1/β-catenin signalling pathway. *Pharm Biol*. 2023;61(1):1364–1373. doi:10.1080/13880209.2023.2249061
11. Zhao N, Wang Y, Ma Y, et al. Jia-Wei-Si-Miao-Yong-An decoction modulates intestinal flora and metabolites in acute coronary syndrome model. *Front Cardiovascu Med*. 2023;9:1038273. doi:10.3389/fcvm.2022.1038273
12. Zhang F, Li Z, Gao P, et al. HJ11 decoction restrains development of myocardial ischemia-reperfusion injury in rats by suppressing ACSL4-mediated ferroptosis. *Front Pharmacol*. 2022;13:1024292. doi:10.3389/fphar.2022.1024292

13. Duttaroy AK. Role of gut microbiota and their metabolites on atherosclerosis, hypertension and human blood platelet function: a review. *Nutrients*. 2021;13(144):144. doi:10.3390/nu13010144
14. Libby P. Inflammation in atherosclerosis—no longer a theory. *Clin Chem*. 2021;67(1):131–142. doi:10.1093/clinchem/hvaa275
15. Kong P, Cui Z-Y, Huang X-F, Zhang -D-D, Guo R-J, Han M. Inflammation and atherosclerosis: signaling pathways and therapeutic intervention. *Signal Transduction Targeted Therap*. 2022;7(1):131. doi:10.1038/s41392-022-00955-7
16. Vourakis M, Mayer G, Rousseau G. The role of gut microbiota on cholesterol metabolism in atherosclerosis. *Int J Mol Sci*. 2021;22(15):8074. doi:10.3390/ijms22158074
17. Di Vincenzo F, Del Gaudio A, Petito V, Lopetuso LR, Scaldaferri F. Gut microbiota, intestinal permeability, and systemic inflammation: a narrative review. *Int Emerg Med*. 2024;19(2):275–293. doi:10.1007/s11739-023-03374-w
18. Jonsson AL, Bäckhed F. Role of gut microbiota in atherosclerosis. *Nat Rev Cardiol*. 2017;14(2):79–87. doi:10.1038/nrcardio.2016.183
19. Meng Q, Bi Y, Feng H, et al. Activation of estrogen receptor α inhibits TLR4 signaling in macrophages and alleviates the instability of atherosclerotic plaques in the postmenopausal stage. *Int Immunopharmacol*. 2023;116:109825. doi:10.1016/j.intimp.2023.109825
20. Fanqi K, Bozhi Y, Jiatian C, et al. Curcumin represses NLRP3 inflammasome activation via TLR4/MyD88/NF-κB and P2X7R signaling in PMA-induced macrophages. *Front Pharmacol*. 2016;7(369).
21. Wang J, Xu P, Xie X, et al. DBZ (Danshensu Bingpian Zhi), a novel natural compound derivative, attenuates atherosclerosis in apolipoprotein E–Deficient mice. *J Am Heart Assoc*. 2017;6(10):e006297.
22. Li T, Li D, Xu H, Zhang H, Tang D, Cao H. Wen-Xin Decoction ameliorates vascular endothelium dysfunction via the PI3K/AKT/eNOS pathway in experimental atherosclerosis in rats. *BMC Complementary Alternat Med*. 2016;2016.
23. Hu X, Xia K, Dai M, et al. Intermittent fasting modulates the intestinal microbiota and improves obesity and host energy metabolism. *Npj Biofilms Microbiomes*. 2023;9(1). doi:10.1038/s41522-023-00386-4
24. Yu H, Li Y, Tao L, et al. Trajectories of lipid profile and risk of carotid atherosclerosis progression: a longitudinal cohort study. *Nutrients*. 2022;14(15):3243. doi:10.3390/nu14153243
25. Linton MF, Yancey PG, Tao H, Davies SS. HDL function and atherosclerosis: reactive dicarbonyls as promising targets of therapy. *Circul res*. 2023;132(11):1521–1545. doi:10.1161/CIRCRESAHA.123.321563
26. Zhou M, Xu H, Liu W, Liu H. Rosiglitazone modulates collagen deposition and metabolism in atherosclerotic plaques of fat-fed ApoE-knockout mice. *Exp Ther Med*. 2015;10(4):1265–1270. doi:10.3892/etm.2015.2711
27. Adachi Y, Ueda K, Nomura S, et al. Beiging of perivascular adipose tissue regulates its inflammation and vascular remodeling. *Nat Commun*. 2022;12(1).
28. Zheng Y, Li Y, Ran X, et al. Mettl14 mediates the inflammatory response of macrophages in atherosclerosis through the NF-κB/IL-6 signaling pathway. *Cell Mol Life Sci*. 2022;79(6):311. doi:10.1007/s00018-022-04331-0
29. Chinetti-Gbaguidi G, Colin S, Staels B. Macrophage subsets in atherosclerosis. *Nat Rev Cardiol*. 2015;12(1):10–17. doi:10.1038/nrcardio.2014.173
30. McArdle S, Buscher K, Ghosheh Y, et al. Migratory and dancing macrophage subsets in atherosclerotic lesions. *Circul res*. 2019;125(12):1038–1051. doi:10.1161/CIRCRESAHA.119.315175
31. Heo J, Kang H. Exosome-based treatment for atherosclerosis. *Int J Mol Sci*. 2022;23(2):1002. doi:10.3390/ijms23021002
32. Shi L, Li Y, Xu X, et al. Brown adipose tissue-derived Nrg4 alleviates endothelial inflammation and atherosclerosis in male mice. *Nat Metab*. 2022;4(11):1573–1590. doi:10.1038/s42255-022-00671-0
33. Shen D-Z, Xin S-L, Chen C, Liu T. Effect of atorvastatin on expression of TLR4 and NF-κB p65 in atherosclerotic rabbits. *Asian Pac J Trop Med*. 2013;6(6):493–496. doi:10.1016/S1995-7645(13)60081-4
34. Liang X, Xiu C, Liu M, et al. Platelet-neutrophil interaction aggravates vascular inflammation and promotes the progression of atherosclerosis by activating the TLR4/NF-κB pathway. *J Cell Biochem*. 2019;120(4):5612–5619. doi:10.1002/jcb.27844
35. Nie H, Xiong Q, Lan G, et al. Sivelestat alleviates atherosclerosis by improving intestinal barrier function and reducing endotoxemia. *Front Pharmacol*. 2022;13:838688. doi:10.3389/fphar.2022.838688
36. Chen Y, Hao Z, Zhao H, et al. Berberine alleviates intestinal barrier dysfunction in glucolipid metabolism disorder hamsters by modulating gut microbiota and gut-microbiota-related tryptophan metabolites. *J Sci Food Agric*. 2023;103(3):1464–1473. doi:10.1002/jsfa.12242
37. Ren K, Jiang T, Zhou H-F, Liang Y, Zhao G-J. Apigenin retards atherogenesis by promoting ABCA1-mediated cholesterol efflux and suppressing inflammation. *Cell Physiol Biochem*. 2018;47(5):2170–2184. doi:10.1159/000491528
38. Lu F, Zou J, Xu W, et al. Mechanism of HJ11 decoction in the treatment of atherosclerosis based on network pharmacology and experimental validation. *Combinatorial Chem Amp*. 2025;28(19):3414–3429. doi:10.2174/0113862073356770241218065012
39. Zhang S, Chen Q, Jin M, et al. Corrigendum to "Notoginsenoside R1 alleviates cerebral ischemia/reperfusion injury by inhibiting the TLR4/MyD88/NF-κB signaling pathway through microbiota-gut-brain axis" [Phytomedicine 128 (2024) 155530]. *Phytomedicine*. 2025;141.

Journal of Inflammation Research

Dovepress
Taylor & Francis Group

Publish your work in this journal

The Journal of Inflammation Research is an international, peer-reviewed open-access journal that welcomes laboratory and clinical findings on the molecular basis, cell biology and pharmacology of inflammation including original research, reviews, symposium reports, hypothesis formation and commentaries on: acute/chronic inflammation; mediators of inflammation; cellular processes; molecular mechanisms; pharmacology and novel anti-inflammatory drugs; clinical conditions involving inflammation. The manuscript management system is completely online and includes a very quick and fair peer-review system. Visit http://www.dovepress.com/testimonials.php to read real quotes from published authors.

Submit your manuscript here: https://www.dovepress.com/journal-of-inflammation-research-journal